Sensors and Actuators B 245 (2017) 238–246

Contents lists available at ScienceDirect

Sensors and Actuators B: Chemical

journal homepage: www.elsevier.com/locate/snb

A novel electrochemical sensor for highly sensitive detection of bisphenol A based on the hydrothermal synthesized Na-doped WO_3 nanorods

Yuanzhen Zhou*, Lehui Yang, Shanghui Li, Yuan Dang

School of Science, Xi'an University of Architecture and Technology, Xi'an, 710055, China

ARTICLE INFO

Article history:
Received 19 August 2016
Received in revised form 4 January 2017
Accepted 5 January 2017
Available online 21 January 2017

Keywords:
Na-doped WO_3 nanorods
Electrocatalytic properties
Electrochemical sensor
Bisphenol A

ABSTRACT

Na-doped WO_3 nanorods were successfully prepared via a hydrothermal synthesis method and further characterized by X-ray diffraction (XRD), scanning electron microscopy (SEM) and energy dispersive X-ray spectroscopy (EDS). A novel and sensitive electrochemical sensor has been fabricated for determination of bisphenol A (BPA) based on the as-synthesized nanomaterials modified carbon paste electrode (CPE). Electrochemical impedance spectroscopy (EIS), cyclic voltammetry (CV) and differential pulse voltammetry (DPV) were applied to demonstrate the electrochemical performances of the Na-doped WO_3 modified CPE (Na-doped WO_3/CPE). By using the DPV technology, the linear calibration curve was obtained within a wide concentration range from 0.0810 μmol L^{-1} to 22.5 μmol L^{-1} with the low detection limit of 0.028 μmol L^{-1} ($S/N = 3$) for BPA. Moreover, the sensor also showed good anti-interference ability in the interference study and satisfactory recovery between 95.70% and 105.3% in the practical sample analysis. Thus, the proposed sensor could be advantageously employed for the determination of BPA in environmental science.

1. Introduction

Bisphenol A (BPA) [4,4′-(propane-2, 2-diyl) diphenol] is one of the widely used industrial raw materials during the production of polycarbonate plastics, epoxy resins, flame retardants and other specialty products [1]. However, a great attention has been paid to the toxicity of BPA for its sustained release from polycarbonate flasks [2], food cans [3,4] and dental products [5] during use. Previous studies have found that BPA has estrogens-like functionality and is an environmental endocrine disrupting chemical (EDC). Even small amount of BPA exposure will induce diverse harmful health effects including diabetes [6], hepatic disease [7], cancer [8], metabolic disease [9] and reproductive health [10]. Therefore, it is urgently needed to develop a highly sensitive and rapid determination method for trace amount of BPA in the environmental monitoring and food safety related fields.

Until now, various analytical methods based on capillary electrophoresis [11], gas chromatography coupled with mass spectrometry (GC–MS) [12], high performance liquid chromatography (HPLC) [13], high performance liquid chromatography coupled with mass spectrometry (HPLC–MS) [14], chemiluminescence detection [15] and enzyme linked immunosorbent assay [16] have been built to determinate BPA. Although the aforementioned techniques are sensitive and effective enough for the determination of BPA, there still are several drawbacks to overcome, such as expensive instrumentation, time-consuming process, strict pretreatments requirements and well-trained operators. Compared with these methods, nowadays, electrochemical sensors have attracted considerable attentions due to their high sensitivity, good selectivity, low cost, fast response, timesaving, convenient operation and on-site monitoring [17]. Nevertheless, the bare electrodes can't attain sensitive detection of BPA because of the poor electron transfer capacity between the sensing interface and BPA. To address this issue, it is very essential to develop favorable materials for surface modification of bare electrodes.

In recent years, with the rapid development of nanoscience, nanomaterials exhibited unique photonic, magnetic, electronic and catalytic properties [18–20] for their particular morphologies and large surface area. Therefore, a wide variety of nanomaterials have been successfully employed to enhance the electrochemical properties of bare electrodes in sensing and catalysis, such as boron-doped diamond nanorods [21], platinum-polydopamine@SiO_2 nanocomposite [22], chitosan/ionic

* Corresponding author at: School of Science, Xi'an University of Architecture and Technology, No. 13, Yant Road, Xi'an, Shaanxi Province, China.
E-mail addresses: zyz1289@126.com, zhouyuanzhen@xauat.edu.cn (Y. Zhou).

http://dx.doi.org/10.1016/j.snb.2017.01.034
0925-4005/

liquid/multiwall carbon nanotubes composite [23], Fe_3O_4 nanoparticle/multiwall carbon nanotube [24], etc. Among the numerous nanoscaled materials, nanostructured tungsten oxides (WO_3) has caused extensive concern on account of its large surface areas, high-aspect-ratio structure, low cost and high electrical conductivity [25,26]. Furthermore, WO_3 presented in several different morphologies with different properties and was extensively applied in various fields including photocatalysts [27], gas sensors [28], field-emission devices [29], electrochromic devices [30], and solar-energy devices [31,32]. However, studies showed that the performance of pure WO_3 was relatively poor. Dong et al. prepared the Pt/WO_3-carrier and successfully improved photocatalytic property of WO_3 [33]. Sn doping effectively enhanced the optical, electrical and anticancer properties of WO_3 [34]. So various strategies, including passivation layer modifying [35], coupled with conducting polymers [36], morphologies controlling [37] and ion doping [38], have been tried to further reinforce the activity of WO_3. Among the above methods, the ion doping was very noteworthy for its easy-operation and remarkable effect. Based on this, a spate of reports on doping some metal ions to achieve the desirable properties of WO_3 emerged [39,40].

Researches have revealed that the alkali metal ions, especially for sodium (Na) doping, can significantly improve the physical and chemical properties of materials. The participation of Na can generate the superbase sites, and the obtained electrons by Na to the oxide lattice usually reside in defect sites [41]. Wang et al. found that Na-doped Cu_2ZnSnS_4 increased the conductivity and conversion efficiency of Cu_2ZnSnS_4 solar cells [42]. Wang et al. showed that Na-doped electrodes possessed of higher initial coulombic efficiency, superior rate capability and better capacity retention by electrochemical testing [43]. From these researches, it can be seen clearly that Na doping is able to greatly strengthen the catalytic and electrochemical properties of nanomaterials. Therefore, the Na-doped WO_3 has great potential to be employed as a better catalytic active material.

In the present work, we synthesized the Na-doped WO_3 nanorods by a hydrothermal synthesis method and developed a sensitive and convenient electrochemical sensor based on as-prepared nanomaterials modified carbon paste electrode (CPE) for the determination of BPA. The electrocatalytic properties of the sensor were characterized by electrochemical impedance spectroscopy (EIS), cyclic voltammetry (CV) and differential pulse voltammetry (DPV). The proposed Na-doped WO_3 modified CPE (Na-doped WO_3/CPE) sensor provides a novel method for sensitive detection of BPA, and has potential applications in determination of environmental samples.

2. Experimental

2.1. Reagents and materials

Sodium tungstate dehydrate ($Na_2WO_4{\cdot}2H_2O$) and oxalic acid ($H_2C_2O_4$) were purchased from Sinopharm Chemical Reagent Co., Ltd. (Shanghai, China). Sodium chloride (NaCl) was gained from Tianjin Kermel Chemical Reagent Co., Ltd. (Tianjin, China). $K_3[Fe(CN)_6]$ and $K_4[Fe(CN)_6]$ were purchased from Tianjin Hongyan Chemical Reagent Factory (Tianjin, China). BPA was purchased from Tianjin Fuchen Chemical Reagent Factory (Tianjin, China). The standard stock solution of 2.00 mmol L^{-1} BPA was prepared by 50% (v/v) ethanol solution. 0.1 mol L^{-1} phosphate buffered solutions (PBS) with different pH values (3.0–9.0) were prepared by mixing KH_2PO_4 and K_2HPO_4 stock solution and adjusting the pH with 1 mol L^{-1} H_3PO_4 and 1 mol L^{-1} KOH. All reagents were of analytical grade and used without further purification. Solutions were prepared using double distilled water except where indicated.

2.2. Apparatus

All electrochemical measurements were performed using a CHI660D electrochemical workstation (Chenhua Instruments, Shanghai, China) with a conventional three-electrode system. A modified (bare) CPE was used as a working electrode, with a saturated calomel electrode and a platinum wire electrode as reference electrode and counter-electrode, respectively. Measurements of pH were carried out by Mettler Toledo Delta 320 pH meter (Shanghai, China). The morphologies of materials and electrodes were obtained using a Hitachi S-3400 scanning electron microscope (SEM). X-ray diffraction (XRD) patterns of WO_3 and Na-doped WO_3 were collected by a Rigaku D/max 2550.

2.3. Synthesis of the pure WO_3 and Na-doped WO_3

The pure WO_3 and Na-doped WO_3 were synthesized by referring to the reported literature [44]. Typically, the synthesis procedure was completed as below. 0.02 mol $Na_2WO_4{\cdot}2H_2O$ was dissolved in distilled water under constant stirring and pH was tuned to 1.0 with dilute hydrochloric acid solution by drops. After stirring for 1 h, mixed 0.02 mol $H_2C_2O_4$ and the white precipitate was redissolved. Then, 0.0117 g NaCl was added to as-obtained solution. The final solution was transferred into teflon lined steel autoclave and kept the sustaining stirring at 180 °C for 24 h. The resulting product was centrifuged and washed with double distilled water several times. Finally, the Na-doped WO_3 sample was obtained by drying at 80 °C for 12 h in the atmosphere of N_2 gas. The synthesis procedures of the pure WO_3 were the same as those for the Na-doped WO_3 except for the absence of NaCl.

2.4. Preparation of modified carbon paste electrode

The bare CPE (Φ = 3.0 mm) was prepared according to the method described in our previous literature [45]. Graphite powder and paraffin oil were hand-mixed at the ratio of 5:0.7 (w/w) to form a homogeneous paste. And then the prepared carbon paste was packed into a PVC tube (Φ = 3.0 mm). A copper wire was inserted into the carbon paste for electrical contact. After fabrication, the CPE was polished mechanically with weighing paper and then cleaned by doubly distilled water. The bare CPE should be scanned at a scan rate of 100 mV s^{-1} in pH 7.0 PBS until a steady state voltammogram appeared for the subsequent preparation of modified electrodes. The electrochemical pre-treatments of WO_3 modified CPE (WO_3/CPE) and Na-doped WO_3/CPE were the same as that of the bare CPE. These two modified electrodes were fabricated according to the procedure of Zheng and his co-workers [46]. Briefly, 0.5 mg Na-doped WO_3 powder was placed on a piece of weight paper, and then made the CPE gently rub over the samples until all of the powder adhered to the CPE surface. The WO_3/CPE was prepared under the same experimental process.

2.5. Electrochemical measurements procedure

EIS measurements were carried out in 5.0 mmol L^{-1} $K_3[Fe(CN)_6]/K_4[Fe(CN)_6]$ mixture by a ratio of 1-to-1 containing 0.1 mol L^{-1} KCl, with the frequencies swept from 10 mHz to 100 kHz. The applied perturbation amplitude in experiment was 5 mV. CV measurements were applied from −0.4 to 0.8 V in $[Fe(CN)_6]^{3-/4-}$ solution and performed from 0.1 to 0.9 V in BPA solution at the scan rate of 100 mV s^{-1}. DPV was measured from 0.1 to 0.8 V at pulse width of 0.05 s and amplitude of 50 mV. All the electrochemical experiments were implemented in a very clean environment to keep the qualities of nanomaterials, electrodes and solutions. Each electrode was stored at room temperature.

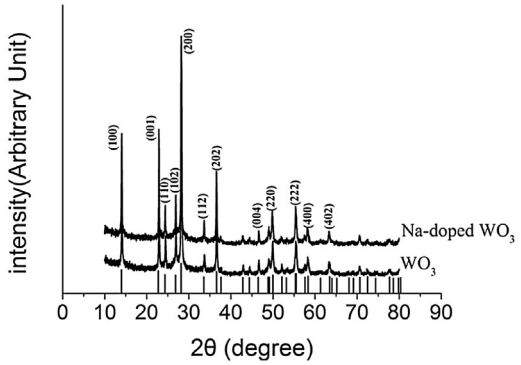

Fig. 1. XRD pattern of the WO_3, Na-doped WO_3 samples and the JCPDS peak for the WO_3 (no.33-1387).

3. Results and discussion

3.1. Crystal structure analysis

The crystal structures of pure WO_3 and Na-doped WO_3 samples were explored by using XRD and the results were shown in Fig. 1. As shown in Fig. 1, all of the prepared samples were highly crystalline and the diffraction peaks were consistent with the hexagonal structured WO_3 (JCPDS no. 33-1387). There was no signal of additional impurity phase pattern pertaining to Na or its oxide in the Na-doped WO_3 sample, which may be related with the Na doping in WO_3 lattice. Diffraction peaks of all the samples were almost the same to each other, corresponding to the following planes: (100), (001), (110), (102), (200), (112), (202), (004), (220), (222), (400) and (402), respectively [47]. Moreover, it was reported that the large

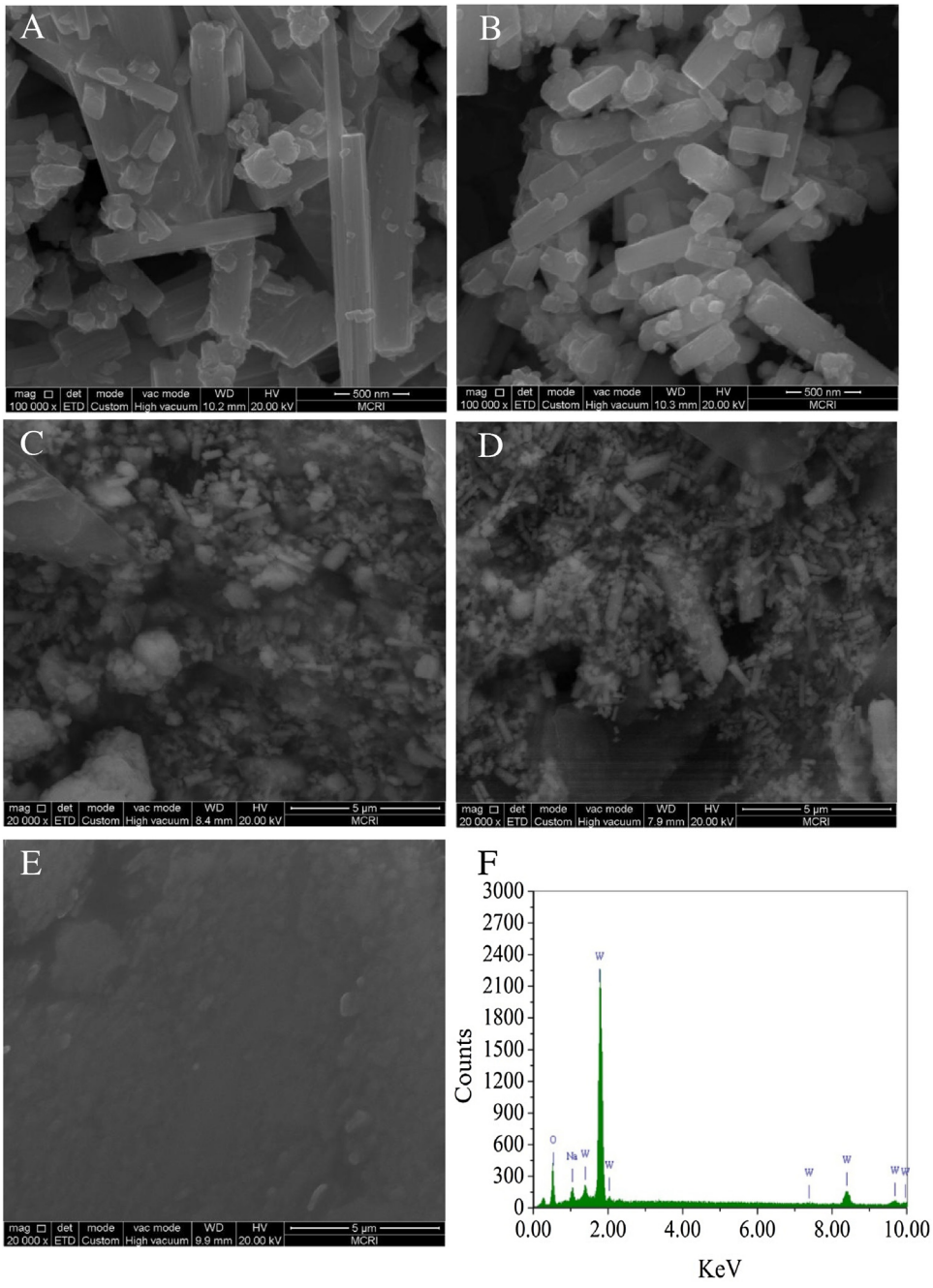

Fig. 2. SEM images of WO_3 (A), Na-doped WO_3 (B), WO_3/CPE (C), Na-doped WO_3/CPE (D) and bare CPE (E) with EDS image of Na-doped WO_3 (F).

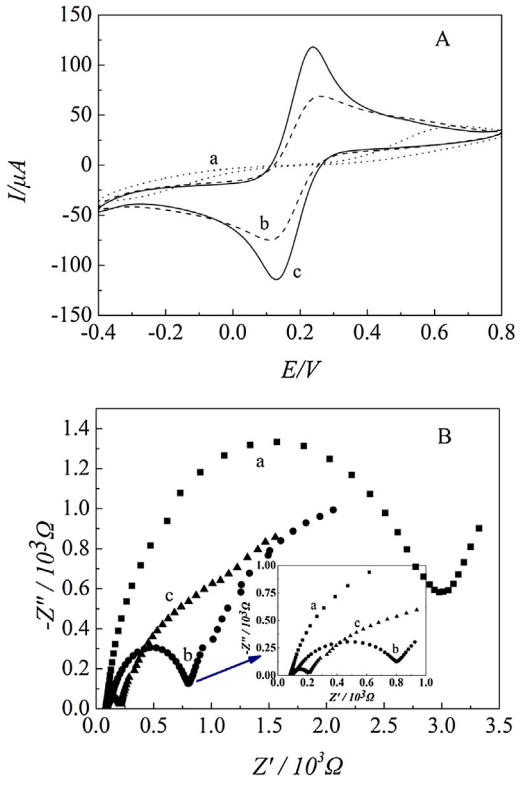

Fig. 3. CVs (A) and Nyquist diagrams of EIS (B) of bare CPE (a), WO_3/CPE (b) and Na-doped WO_3/CPE (c) in the solution of 5.0 mmol L^{-1} $[Fe(CN)_6]^{3-/4-}$ (1:1) and 0.1 mol L^{-1} KCl. CVs were recorded at a scan rate of 100 mV s^{-1}; Nyquist plots were obtained at the frequencies swept from 10^5 to 10^{-2} Hz at the formal potential of the redox couple.

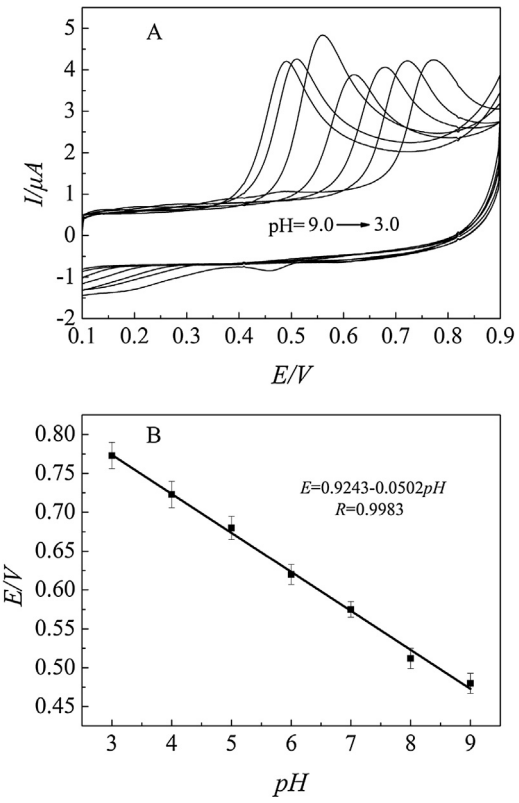

Fig. 5. (A) CVs recorded with Na-doped WO_3/CPE in different pH: 3.0, 4.0, 5.0, 6.0, 7.0, 8.0, and 9.0 containing 5.0×10^{-6} mol L^{-1} BPA; (B) Calibration plot showed effects of pH on peak potentials at Na-doped WO_3/CPE.

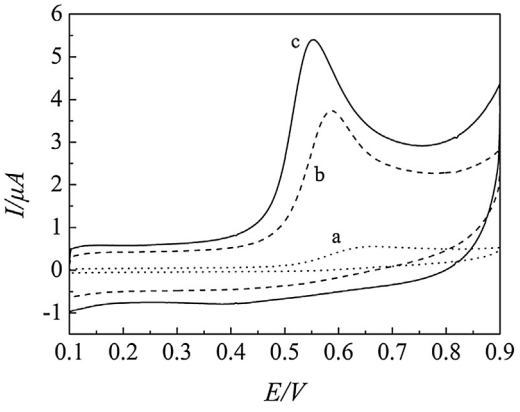

Fig. 4. CVs of 5.0×10^{-6} mol L^{-1} BPA at a bare CPE (a), WO_3/CPE (b) and Na-doped WO_3/CPE (c) in 0.1 mol L^{-1} PBS (pH 7.0) with the scan rate of 100 mV s^{-1}.

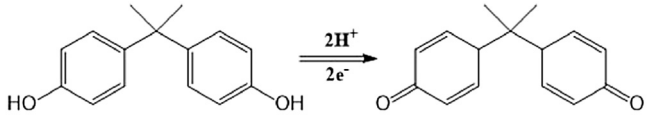

Scheme 1. Possible reaction of BPA oxidation on the Na-doped WO_3/CPE.

tunnels were formed by octahedral sharing (WO_6) in the hexagonal structured WO_3 [48]. Hence, the ions can be easily embedded into these tunnels and Na ions can substitute into the interstitial sites of the hexagonal WO_3 successfully.

3.2. Morphological characterization

SEM was employed to investigate the nanostructures and morphologies of the as-prepared samples and electrodes. The SEM images of undoped WO_3, Na-doped WO_3 and modified electrodes were displayed in Fig. 2. It exhibited remarkable heterogeneous and agglomerate rod like shape in the undoped WO_3 (Fig. 2A). Meanwhile, in Fig. 2B, Na-doped WO_3 was composed of many nanorods with average diameter of about 100 nm and length range of 0.5–1 μm. This 1D structure was advantageous for the electrochemical catalysis due to the charges could be transferred in direct ways [49]. Therefore, the Na-doped WO_3 nanorods might enhance the interaction between BPA and modified electrode to further facilitate the electrochemical properties of Na-doped WO_3/CPE. In order to evaluate the elementary composition of the obtained Na-doped WO_3 sample, the energy dispersive X-ray spectroscopy (EDS) was analyzed and the result was displayed in Fig. 2F. It could be seen that multiple well-defined peaks were observed clearly corresponding to O, W and Na with no other impurities peaks. The content of Na was determined to be 5at%. These consequences further revealed the successful formation of Na-doped WO_3 and verified the aforementioned prediction that the Na doping in WO_3 lattice. Additionally, the surface morphologies comparison between bare CPE and different modified electrodes showed that the presence of nanostructure materials was well evidenced. The bare CPE (Fig. 2E)shaped irregularly with isolated graphite flakes and distinguished layers. But for the modified electrodes, nanomaterials covered the CPE surface massively and arranged randomly as shown in Fig. 2C and 2D, which confirmed that WO_3 and Na-doped WO_3 nanorods adhered successfully to the bare CPE to form more active WO_3/CPE and Na-doped WO_3/CPE.

3.3. Electrochemical properties of the modified electrodes

Electrochemical characterizations of the electrodes were investigated by CV with the probe of $[Fe(CN)_6]^{3-/4-}$. Fig. 3A showed the CVs of bare CPE (a), WO_3/CPE (b) and Na-doped WO_3/CPE (c) in 5.0 mmol L^{-1} $[Fe(CN)_6]^{3-/4-}$ solution containing 0.1 mol L^{-1} KCl at the scan rate of 100 mV s^{-1}. It can be seen that a pair of redox peaks with poor symmetry were obtained with peak-to-peak separation (ΔE_p) about 890 mV at bare CPE (curve a). While at the WO_3/CPE (curve b), the CV responses of ΔE_p declined obviously to 170 mV, indicating that WO_3 could greatly increase the electron transfer rate between $[Fe(CN)_6]^{3-/4-}$ and electrode surface. In the meantime, a pair of well-defined redox peaks were observed at the Na-doped WO_3/CPE (curve c) with a further decreasing ΔE_p of 110 mV and significantly enhancing redox peak currents, indicating the better electrochemical reversibility than that of bare CPE and WO_3/CPE. Meanwhile, the electroactive surface of modified electrode was investigated. According to the Randles ~ Sevick equation: $i_p = 2.69 \times 10^5 n^{3/2} A D^{1/2} v^{1/2} C$, the result showed that the electroactive surface of Na-doped WO_3/CPE was 1.3 times that of WO_3/CPE. These phenomena indicated Na-doped WO_3 nanorods could effectively promote the electron transfer rate and had the preferable catalysis performance than WO_3.

EIS was used for characterization of the interface electron transfer capabilities of different electrodes. As displayed in Fig. 3B, the different Nyquist plots about (a) bare CPE, (b) WO_3/CPE and (c) Na-doped WO_3/CPE were achieved in the same $[Fe(CN)_6]^{3-/4-}$ solution mentioned above. The charge transfer resistance (R_{ct}) at the electrode surface is equal to the semicircle diameter. In curve a, a large diameter was obtained at the bare CPE (R_{ct} = 3000 Ω), which indicated a very poor electron transfer process. However, the semicircle diameter obviously diminished (R_{ct} = 800 Ω) when WO_3 was modified to the surface of bare CPE (curve b), implying that WO_3 facilitated the electron transfer from $[Fe(CN)_6]^{3-/4-}$ to the electrode surface. Meanwhile, on the Na-doped WO_3/CPE (curve c), the R_{ct} value sharply reduced to 210 Ω, which was lower than that for WO_3/CPE and bare CPE. These results proved that WO_3 and Na-doped WO_3 were successfully accreted on bare CPE surface and the Na-doped WO_3 was a particularly effective medium to enhance the conductivity of the electrode and enhanced the electron transfer rate between the solution and electrode surface.

3.4. Electrocatalytic behaviors of Bisphenol A

Fig. 4 showed the CVs of 5.0×10^{-6} mol L^{-1} BPA in 0.1 mol L^{-1} PBS (pH 7.0) at bare CPE, WO_3/CPE and Na-doped WO_3/CPE at a scan rate of 100 mV s^{-1}, respectively. At bare CPE (curve a), the oxidation of BPA occurred at the high potential of 0.665 V with weak current response (0.432 μA). While at WO_3/CPE (curve b), a well-defined oxidation peak of BPA appeared at 0.587 V with an enhanced oxidation current (3.124 μA), suggesting WO_3 was helpful to improve the catalytic process of BPA. Moreover, the Na-doped WO_3/CPE (curve c) provided a greater peak current about 4.664 μA which was around 1.5 times that of WO_3/CPE and 11 times of bare CPE. What is more, the peak potential shifted negatively to 0.553 V. These results suggested that Na-doped WO_3 could accelerate the electrocatalytic oxidation of BPA, which might be attributed to the successful introduction of Na and the unique characteristics of Na-doped WO_3 such as high effective specific surface area and better electric conductivity. Moreover, Na-doped WO_3/CPE had the bigger electroactive electrode surface.

3.5. Effects of solution pH

It is noted that the pH of the electrolyte has a profound influence on the electrochemical behaviour of BPA. The effect of pH on the electrochemical properties of Na-doped WO_3/CPE toward 5.0×10^{-6} mol L^{-1} BPA was investigated by CV (Fig. 5A). A series of well-defined oxidation peaks of BPA appeared in the pH range from 3.0 to 9.0. As can be seen, the oxidation peak current at pH 7.0 was in a state of the maximum value. The pH of maximum response was lower than the *pKa* of BPA (*pKa* = 9.73) [50], indicating that the undissociated BPA could adsorb better than the dissociated BPA on the Na-doped WO_3/CPE surface. Therefore, PBS with the pH of 7.0 was selected as the supporting electrolyte for the desirable sensitivity of the determination of BPA. Additionally, the relationship of pH value vs. peak potential was studied in Fig. 5B. It was found that the oxidation peak potentials shifted linearly to the negative direction with the increase of pH and it obeyed the following equation, $E(V) = (0.9243 \pm 0.0096) - (0.0502 \pm 0.0014)pH$ (R = 0.9983). The slope value of 50.2 mV per pH was approximately to the theoretical value of 57.6 mV per pH [51]. The fact revealed that the oxidation process of BPA on Na-doped WO_3/CPE surface accompanied an equal number of electrons and protons transfer process.

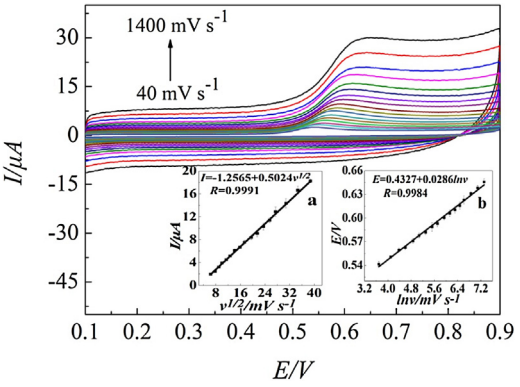

Fig. 6. CVs of 5.0×10^{-6} mol L^{-1} BPA on Na-doped WO_3/CPE at different scan rates: 40, 60, 80, 100, 130, 160, 200, 250, 300, 380, 460, 550, 650, 750, 950, 1200, and 1400 mV s^{-1}. Inset: (a) the plot of the oxidation peak current (I) versus the square root of scan rate ($v^{1/2}$) and (b) the relationship between the peak potential (E) and natural logarithm of scan rate (lnv). Supporting electrolyte was 0.1 mol L^{-1} PBS of pH 7.0.

3.6. Effects of scan rate

To assess the electrocatalytic mechanism of Na-doped WO_3/CPE, CVs of 5.0×10^{-6} mol L^{-1} BPA at different scan rates of 40–1500 mV s^{-1} were recorded in Fig. 6. It could be clearly seen that the oxidation peaks of BPA shifted to positive potentials and the oxidation peak currents also gradually increased with the increasing of scan rates. The inset (a) exhibited that the oxidation peak current (I) of BPA was linearly proportional to the square root of scan rate ($v^{1/2}$), and the linear regression equation can be estimated as $I(\mu A) = (0.5024 \pm 0.0063)v^{1/2} - (1.2565 \pm 0.0538)$ (R = 0.9991). The results indicated that the oxidation of BPA on Na-doped WO_3/CPE surface was controlled by diffusion process [52]. Meanwhile, a good linear relationship between the oxidation peak potential (E) and natural logarithm of scan rate (lnv) was also obtained in the inset (b). The equation was $E = (0.0286 \pm 0.0005)lnv + (0.4327 \pm 0.0024)$ (R = 0.9984). As for an electron-controlled and totally irreversible electrode process, the E was defined by the following equation [51]:

$$E = E^{\theta} + \left(\frac{RT}{\alpha nF}\right) \ln\left(\frac{RTk^{\theta}}{\alpha nF}\right) + \left(\frac{RT}{\alpha nF}\right) \ln v$$

Where α, k^{θ}, n, v, E^{θ}, R, T, and F represent transfer coefficient, standard rate constant of the reaction, electron transfer number

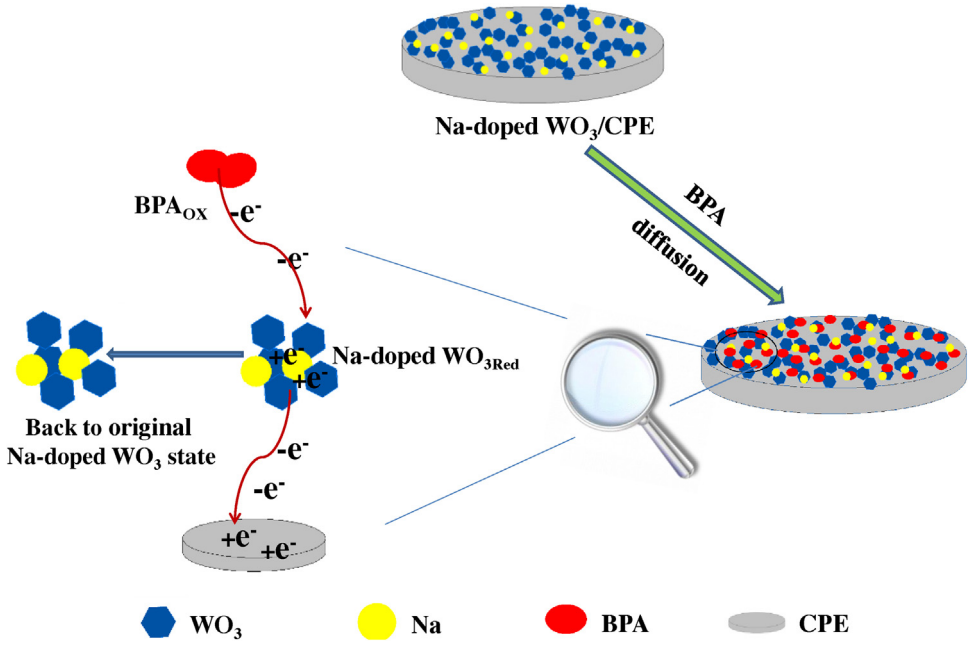

Fig. 7. Possible catalytic mechanism of the electrochemical sensor.

involved in rate determining step, scan rate, formal redox potential, the gas constant, the absolute temperature and the Faraday constant, respectively. According to the linear correlation of E versus lnv as mentioned above, the slope was equal to $RT/\alpha nF$. Generally, α is assumed to be 0.5 in totally irreversible electrode process [53], so the n was calculated to be 1.79 (taking $T = 298$, $R = 8.314$, and $F = 96480$). Considering the fact that the number of electron and proton participating in the oxidation process of BPA was equal, demonstrated in Section 3.5, the electrocatalytic oxidation of BPA at Na-doped WO_3/CPE may be a two-electron and two-proton process. The possible oxidation process was predicted and illustrated in Scheme 1:

The possible mechanism of the electrocatalytic process was speculated and showed in Fig. 7. As shown in Fig. 7, at the beginning of oxidation process, a large amount of BPA molecules diffused into the surface of Na-doped WO_3/CPE to form the transition state complexes [54]. With the increasing potential loaded on the electrode, BPA was oxidized to the quinoid structure and Na-doped WO_3 was changed into the reduction state by capturing the lost electrons of BPA. The as-reduced nanomaterials transfered electrons continuously to the bare electrode and then the Na-doped WO_3 changed to its original state. Meanwhile, the quinoid structure has been in the stable state. In the whole reaction process, the Na-doped WO_3 nanorods were an important medium to increase the concentration of the free electrons and decrease the energy barrier that electrons directly passed from BPA to bare CPE surface, which eventually enhanced the conductivity of the proposed sensor. The result suggested that Na-doped WO_3/CPE was an useful tool towards the oxidation of BPA with the excellent electrocatalytic activity.

3.7. Analytical performance of the Na-doped WO_3/CPE

DPV was employed to evaluate the analytical performance of the sensor when the Na-doped WO_3/CPE was incubated with various concentrations of BPA solution. As shown in Fig. 8, under the optimal experimental conditions, the oxidation peak currents increased linearly against the concentration of BPA within the range of $0.0810 \sim 22.5\ \mu mol\ L^{-1}$. The resulting linear equation was $I(\mu A) = (0.3105 \pm 0.0102)C + (0.4053 \pm 0.0243)$ ($R = 0.9950$). The detection limit (LOD) was estimated using the expression: kSD_a/b where $k = 3$ for LOD, SD_a is the standard deviation of the intercept and b is the slope of the calibration plot. So the LOD of BPA was estimated to be $0.028\ \mu mol\ L^{-1}$. The experiment result confirmed that the fabricated sensor had wider concentration range, lower detection limit and good sensitivity for the measurements of BPA. A comparison of Na-doped WO_3/CPE with other previously reported modified electrodes for detecting BPA was listed in Table 1. All of the results suggested that the analytical performance of Na-doped WO_3/CPE was essentially comparable to that of other differently types of BPA electrochemical sensors. The prominent electrocatalytic property could be ascribed to the large specific surface area and good electron transfer capability of the Na-doped WO_3 nanorods and the bigger electroactive surface of Na-doped WO_3/CPE. In addition, as compared to the other surface modifiers listed in Table 1, the Na-doped WO_3 nanorods were prepared by a facile hydrothermal synthesis method and the utilized raw materials were inexpensive and easy-to-get. And more importantly, the preparation method of modified electrodes was simple and easy-to-operate. Thus, the Na-doped WO_3/CPE may be potentially applied for monitoring the BPA concentration.

3.8. Stability, reproducibility, repeatability and selectivity

The stability of the sensor was evaluated by repeating DPV measurements at $5.0 \times 10^{-6}\ mol\ L^{-1}$ BPA when Na-doped WO_3/CPE was stored at the room temperature for 5 days. The peak current signals of BPA barely changed in the first day, and retained 94%, 90% and 85% of their original response for the second, third and fifth day, respectively. The result verified that the stability of the Na-doped WO_3/CPE was comparatively ideal. 5 Na-doped WO_3/CPE with the consistent backgrounds were used to examine the $5.0 \times 10^{-6}\ mol\ L^{-1}$ BPA by monitoring the CV responses to evaluate the reproducibility of the prepared sensor. As shown in Fig. 9, the relative standard deviation (RSD) was less than 5%, indicating that the Na-doped WO_3/CPE possessed a good reproducibility. Moreover, one of the aforementioned electrodes was selected to assess the repeatability of Na-doped WO_3/CPE via 16 successive measurements of $5.0 \times 10^{-6}\ mol\ L^{-1}$ BPA by DPV. The RSD of the anodic currents was calculated to be 4.3%, indicating the good repeatability of the proposed sensor. Furthermore,

Table 1
Comparison of the analytical parameters of different modified electrodes for the determination of BPA.

Modified electrode	Linear range (μmol L^{-1})	Detection limit (μmol L^{-1})	Sensitivity μA•(μmol/ L)$^{-1}$	References
MMIPs-CTAB/CPE	0.6–100	0.10	0.61	[55]
MCM-41/CPE	0.22–8.8	0.038	2.833	[56]
CMK-3/nano-CILPE	0.2–150	0.05	0.7741	[57]
Pt/Gr-CNTs/GCE	0.06–10 10–80	0.042	1.156 0.2646	[58]
Thin-film electrode array	0.044–4.4	0.044	0.1085	[59]
AuNPs/SGNF/GCE	0.08–250	0.035	0.06515	[60]
MIP-SiO_2/CPE	0.1–500	0.03222	0.141	[61]
PEDOT/GCE	90–410	55	0.0634	[62]
Na-doped WO_3/CPE	0.0810–22.5	0.028	0.3105	this work

Table 2
The effect of different interferences towards the determination of BPA at Na-doped WO_3/CPE.

Interference	Concentration (mol L^{-1})	Recovery (%)
Mg^{2+}	5.0×10^{-4}	103.9%
Ca^{2+}	5.0×10^{-4}	98.20%
Cu^{2+}	5.0×10^{-4}	95.39%
Fe^{3+}	5.0×10^{-4}	95.06%
NO_3^-	5.0×10^{-4}	97.80%
SO_4^{2-}	5.0×10^{-4}	95.12%
glucose	1.0×10^{-3}	96.51%
sucrose	1.0×10^{-3}	104.1%
fructose	1.0×10^{-3}	98.03%
histidine	5.0×10^{-4}	102.6%
threonine	5.0×10^{-4}	96.13%
alanine	5.0×10^{-4}	95.75%
hydroquinone	2.5×10^{-5}	96.84%
pentachlorophenol	2.5×10^{-5}	95.02%

some foreign substances on the determination of 5.0×10^{-6} mol L^{-1} BPA were investigated to measure the selectivity of the electrochemical sensor. As shown in Table 2, 100-fold concentrations of inorganic ions such as Mg^{2+}, Ca^{2+}, Cu^{2+}, Fe^{3+}, NO_3^- and SO_4^{2-}, did not affect BPA current response (signal change below ±5%). 200-fold concentration of glucose, sucrose and fructose, 100-fold concentration of histidine, threonine and alanine, 5-fold concentrations of hydroquinone and pentachlorophenol, barely influenced the current response of BPA with relative errors less than ±5%. These results indicated that Na-doped WO_3/CPE had an excellent anti-interference ability for some coexisting substances and a good selectivity for BPA detection.

3.9. Real sample analysis

In order to evaluate the practical performance of the proposed BPA sensor, the Na-doped WO_3/CPE was used to determine BPA in the tap water samples and the sterilized milk samples via a recovery study. All tap water samples were collected in the laboratory and used without further treatment. All treated milk samples were employed as the base solutions. These samples were spiked with certain levels of BPA under the optimal experimental conditions. The BPA content in the samples was determined with the previously described procedure by using the spike/recovery test. The results were listed in Table 3. The achieved recoveries of BPA were in the range of 95.70%-105.3%, indicating that the developed Na-doped WO_3/CPE sensor was applicable for BPA detection in practical samples.

4. Conclusion

In this work, a novel rapid detection method towards BPA based on the Na-doped WO_3 nanorods modified electrode has been developed. Na-doped WO_3 nanorods were synthesized by hydrothermal method and applied as effective sensing materials due to its homogeneous nano-scaled size and the special 1D structure, which was benefit to charge transfer. Electrochemical results demonstrated that the Na-doped WO_3/CPE had excellent electrocatalytic activity for BPA oxidation compared with WO_3/CPE and bare CPE. The fabricated sensor exhibited a wide linear response range of 0.0810–22.5 μmol L^{-1}, a low detection limit of 0.028 μmol L^{-1} and

Table 3
Recoveries of BPA from spiked real samples using Na-doped WO_3/CPE.

Samples	Added (μmol L^{-1})	Found (μmol L^{-1})	Recovery (%)
Tap water 1	5	4.832	96.64%
Tap water 2	10	9.903	99.03%
Tap water 3	20	20.84	104.2%
Milk 1	5	5.180	103.6%
Milk 2	10	9.570	95.70%
Milk 3	20	21.05	105.3%

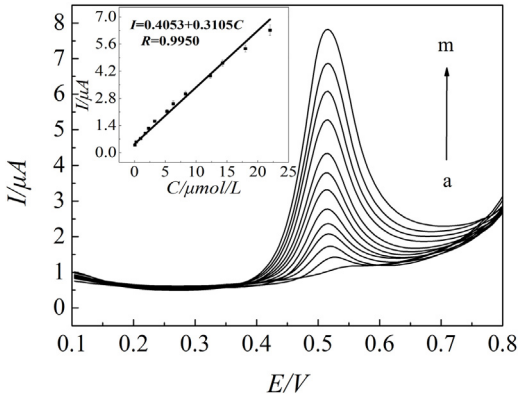

Fig. 8. DPV voltammograms at Na-doped WO_3/CPE for different concentrations BPA in a 0.1 mol L^{-1} PBS (pH 7.0). The concentrations of BPA from a (inner) to m (outer) were 8.10×10^{-8}, 2.91×10^{-7}, 9.91×10^{-7}, 1.79×10^{-6}, 2.29×10^{-6}, 3.29×10^{-6}, 5.29×10^{-6}, 6.29×10^{-6}, 8.29×10^{-6}, 1.23×10^{-5}, 1.43×10^{-5}, 1.83×10^{-5} and 2.25×10^{-5} mol L^{-1}. Insert showed plot of oxidation peak current vs. concentration of BPA.

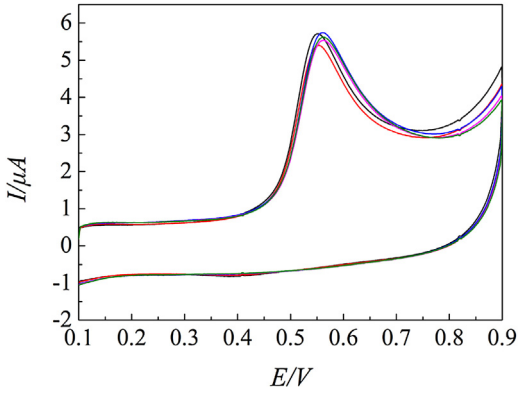

Fig. 9. The reproducibility curve of 5.0×10^{-6} mol L^{-1} BPA on Na-doped WO_3/CPE".

good anti-interference. Additionally, the sensor was successfully applied to real samples with acceptable recovery for the determination of BPA. With these fascinating advantages, the Na-doped WO_3/CPE sensor could be further employed for the electroanalytical and biosensing applications.

Acknowledgments

This work was supported by the Shaanxi Provincial Natural Science Foundation (No. 2014JM2041) and the Open Foundation of Key Laboratory of Synthetic and Natural Functional Molecule Chemistry of Ministry of Education (No. 338080044).

References

[1] C.A. Staples, P.B. Dome, G.M. Klecka, S.T. O'block, L.R. Harris, A review of the environmental fate, effects, and exposures of bisphenol A, Chemosphere 36 (1998) 2149–2173.
[2] A.V. Krishnan, P. Stathis, S.F. Permuth, L. Tokes, D. Feldman, Bisphenol-A: an estrogenic substance is released from polycarbonate flasks during autoclaving, Endocrinology 132 (1993) 2279–2286.
[3] Y. Takao, H.C. Lee, S. Kohra, K. Arizono, Release of bisphenol A from food can lining upon heating, J. Health Sci. 48 (2002) 331–334.
[4] A. Goodson, H. Robin, W. Summerfield, I. Cooper, Migration of bisphenol A from can coatings-effects of damage, storage conditions and heating, Food Addit. Contam. 21 (2004) 1015–1026.
[5] R. Joskow, D.B. Barr, J.R. Barr, A.M. Calafat, L.L. Needham, C. Rubin, Exposures to bisphenol A from bis-glycidyl dimethacrylate-based dental sealants, J. Am. Dent. Assoc. 137 (2006) 353–362.
[6] K.S. Kim, J. Jang, W.S. Choe, P.J. Yoo, Electrochemical detection of bisphenol A with high sensitivity and selectivity using recombinant protein-immobilized graphene electrodes, Biosens. Bioelectron. 71 (2015) 214–221.
[7] R.S. Strakovsky, H. Wang, N.J. Engeseth, J.A. Flaws, W.G. Helferich, Y.X. Pan, S. Lezmi, Developmental bisphenol A (BPA) exposure leads to sex-specific modification of hepatic gene expression and epigenome at birth that may exacerbate high-fat diet-induced hepatic steatosis, Toxicol. Appl. Pharm. 284 (2015) 101–112.
[8] T. Pollock, D. deCatanzaro, Presence and bioavailability of bisphenol A in the uterus of ratsand mice following single and repeated dietary administrationat low doses, Reprod. Toxicol. 49 (2014) 145–154.
[9] B.M. Angle, R.P. Do, D. Ponzi, R.W. Stahlhut, B.E. Drury, S.C. Nagel, W.V. Welshons, C.L. Besch-Williford, P. Palanza, S. Parmigiani, F.S. vom Saal, J.A. Taylor, Metabolic disruption in male mice due to fetal exposure to low butnot high doses of bisphenol A (BPA): Evidence for effects on bodyweight, food intake, adipocytes, leptin, adiponectin, insulin and glucose regulation, Reprod. Toxicol. 42 (2013) 256–268.
[10] P. Wisniewski, R.M. Romano, M.M.L. Kizys, K.C. Oliveira, T. Kasamatsu, G. Giannocco, M.I. Chiamolera, M.R. Dias-da-Silva, M.A. Romano, Adult exposure to bisphenol A (BPA) in wistar rats reduces sperm quality with disruption of the hypothalamic-pituitary-testicular axis, Toxicology 329 (2015) 1–9.
[11] S. Alsudir, Z. Iqbal, E.P.C. Lai, Rapid CE-UV binding tests for selective recognition of bisphenol A by molecularly imprinted polymer particles, Electrophoresis 33 (2012) 1255–1262.
[12] M. Lorber, A. Schecter, O. Paepke, W. Shropshire, K. Christensen, L. Birnbaum, Exposure assessment of adult intake of bisphenol A (BPA) with emphasis on canned food dietary exposures, Environ. Int. 77 (2015) 55–62.
[13] J. Sajiki, K. Takahashi, J. Yonekubo, Sensitive method for the determination of bisphenol-A in serum using two systems of high-performance liquid chromatography, J. Chromatogr. B 736 (1999) 255–261.
[14] S.M. Zimmers, E.P. Browne, P.W. O'Keefe, D.L. Anderton, L. Kramer, D.A. Reckhow, K.F. Arcaro, Determination of free Bisphenol A (BPA) concentrations in breast milk of U.S. women using a sensitive LC/MS/MS method, Chemosphere 104 (2014) 237–243.
[15] E. Maiolini, E. Ferri, A.L. Pitasi, A. Montoya, M.D. Giovanni, E. Errani, S. Girotti, A determination in baby bottles by chemiluminescence enzyme-linked immunosorbent assay, lateral flow immunoassay and liquid chromatography tandem mass spectrometry, Analyst 139 (2014) 318–324.
[16] M. Zhao, Y. Li, Z. Guo, X. Zhang, W. Chang, A new competitive enzyme-linked immunosorbent assay (ELISA) for determination of estrogenic bisphenols, Talanta 57 (2002) 1205–1210.
[17] X.L. Niu, W. Yang, G.Y. Wang, J. Ren, H. Guo, J.Z. Gao, A novel electrochemical sensor of bisphenol A based on stacked graphene nanofibers/gold nanoparticles composite modified glassy carbon electrode, Electrochim. Acta 98 (2013) 167–175.
[18] E. Katz, I. Willner, Integrated nanoparticle-biomolecule hybrid systems: synthesis, properties, and applications, Angew. Chem. Int. Ed. 43 (2004) 6042–6108.
[19] Y.J. Ding, S.S. Wang, J.H. Li, L.X. Chen, Nanomaterial-based optical sensors for mercury ions, TrAC Trends Anal. Chem. 82 (2016) 175–190.
[20] C.L. Lu, Q.M. Shen, X.M. Zhao, J.J. Zhu, X.F. Guo, W.H. Hou, Ag nanoparticles self-supported on $Ag_2V_4O_{11}$ nanobelts: novel nanocomposite for direct electron transfer of hemoglobin and detection of H_2O_2, Sens. Actuators B 150 (2010) 200–205.
[21] D. Luo, L. Wu, J. Zhi, Fabrication of boron-doped diamond nanorod forest electrodes and their application in nonenzymatic amperometric glucose biosensing, ACS Nano 3 (2009) 2121–2128.
[22] J. Manokaran, R. Muruganantham, A. Muthukrishnaraj, N. Balasubramanian, Platinum-polydopamine@SiO_2 nanocomposite modified electrode for the electrochemical determination of quercetin, Electrochim. Acta 168 (2015) 16–24.
[23] Y. Zhang, J.B. Zheng, Direct electrochemistry and electrocatalysis of cytochrome c based on chitosan-room temperature ionic liquid-carbon nanotubes composite, Electrochim. Acta 54 (2008) 749–754.
[24] T. Madrakian, S. Maleki, M. Heidari, A. Afkhami, An electrochemical sensor for rizatriptan benzoate determination using Fe_3O_4 nanoparticle/multiwall carbon nanotube-modified glassy carbon electrode in real samples, Mater. Sci. Eng. C 63 (2016) 637–643.
[25] B.Y. Baek, Y. Song, K. Yong, A Novel Heteronanostructure system: hierarchical W nanothorn arrays on WO_3 nanowhiskers, Adv. Mater. 18 (2006) 3105–3110.
[26] J. Ma, J. Zhang, S. Wang, T. Wang, J. Lian, X. Duan, W. Zheng, Topochemical preparation of WO_3 nanoplates through precursor H_2WO_4 and their gas-Sensing performances, J. Phys. Chem. C 115 (2011) 18157–18163.
[27] S.H. Baeck, K.S. Choi, T.F. Jaramillo, G.D. Stucky, E.W. McFarland, Enhancement of photocatalytic and electrochromic properties of electrochemically fabricated mesoporous WO_3 thin films, Adv. Mater. 15 (2003) 1269–1273.
[28] A. Ponzoni, E. Comini, G. Sberveglieri, J. Zhou, S.Z. Deng, N.S. Xu, Y. Ding, Z.L. Wang, Ultrasensitive and highly selective gas sensors using three-dimensioned tungsten oxide nanowire networks, Appl. Phys. Lett. 88 (2006) 20–22.
[29] J. Zhou, L. Gong, S.Z. Deng, J. Chen, J.C. She, N.S. Xu, R. Yang, Z.L. Wang, Growth and field-emission property of tungsten oxide nanotip arrays, Appl. Phys. Lett. 87 (2005) 223108-1–223108-3.
[30] C. Santato, M. Odziemkowshi, M. Ulmann, J. Augustynski, Crystallographically oriented mesoporous WO_3 films: synthesis, characterization, and applications, J. Am. Chem. Soc. 123 (2001) 10639–10649.
[31] C.G. Granqvist, Electrochromic tungsten oxide films: review of progress 1993–1998, Sol. Energy Mater. Sol. Cells 60 (2000) 201–262.
[32] L. Cheng, Y. Hou, B. Zhang, S. Yang, J.W. Guo, L. Wu, H.G. Yang, Hydrogen-treated commercial WO_3 as an efficient electrocatalyst for triiodide reduction in dye-sensitized solar cells, Chem. Commun. 49 (2013) 5945–5947.
[33] P.Y. Dong, N. Xu, Y. Xu, X.F. Wang, A study of Pt/WO_3-carrier catalysts for photocatalytic purification of NO gas, Catal. Commun. 84 (2016) 142–146.
[34] F. Mehmood, J. Iqbal, T. Jan, W. Ahmed, W. Ahmed, A. Arshad, Q. Mansoor, S.Z. Ilyas, M. Ismail, I. Ahmad, Effect of Sn doping on the structural, optical, electrical and anticancer properties of WO_3 nanoplates, Ceram. Int. 42 (2016) 14334–14341.
[35] W. Kim, T. Tachikawa, D.M. Satoca, H. Kim, T. Majima, W. Choi, Promoting water photo oxidation on transparent WO_3 thin films using an alumina overlayer, Energy Environ. Sci. 6 (2013) 3732–3739.
[36] J.H. Sun, X. Shu, Y.L. Tian, Z.F. Tong, S.L. Bai, R.X. Luo, D.Q. Lia, A.F. Chen, Preparation of polypyrrole@WO_3 hybrids with p-n heterojunction and sensing performance to triethylamine at room temperature, Sens. Actuators B 238 (2017) 510–517.
[37] W. Li, P. Da, Y. Zhang, Y. Wang, X. Lin, X. Gong, G. Zheng, WO_3 nanoflakes for enhanced photoelectrochemical conversion, ACS Nano 8 (2014) 11770–11777.
[38] T. Tesfamichael, A. Ponzoni, M. Ahsan, G. Faglia, Gas sensing characteristics of Fe-doped tungsten oxide thin films, Sens. Actuators B 168 (2012) 345–353.
[39] S.B. Upadhyay, R.K. Mishra, P.P. Sahay, Cr-doped WO_3 nanosheets: structural, optical and formaldehyde sensing properties, Ceram. Int. 42 (2016) 15301–15310.
[40] Z.W. Liu, B. Liu, W.Y. Xie, H. Li, R. Zhou, Q.H. Li, T.H. Wang, Enhanced selective acetone sensing characteristics based on Co-doped WO_3 hierarchical flower-like nanostructures assembled with nanoplates, Sens. Actuators B 235 (2016) 614–621.
[41] H. Matsuhashi, M. Oikawa, K. Arata, Formation of superbase sites on alkaline earth metal oxides by doping of alkali metals, Langmuir 16 (2000) 8201–8205.
[42] W. Xiao, J.N. Wang, X.S. Zhao, J.W. Wang, G.J. Huang, L. Cheng, L.J. Jiang, L.G. Wang, Intrinsic defects and Na doping in Cu_2ZnSnS_4: a density-functional theory study, Sol. Energy 116 (2015) 125–132.
[43] Z.J. Huang, Z.X. Wang, Q. Jing, H.J. Guo, X.H. Li, Z.H. Yang, Investigation on the effect of Na doping on structure and Li-ion kinetics of layered $LiNi_{0.6}Co_{0.2}Mn_{0.2}O_2$ cathode material, Electrochim. Acta 192 (2016) 120–126.
[44] X. Wang, L.X. Pang, X.Y. Hu, N.F. Han, Fabrication of ion doped WO_3 photocatalysts through bulk and surface doping, J. Environ. Sci. 35 (2015) 76–82.
[45] Y.Z. Zhou, H.Y. Zhang, J. Zhang, T. Liu, W.M. Tang, Electrochemically sensitive determination of dopamine and uric acid based on poly (beryllon II)/nanowires-$LaPO_4$ modified carbon paste electrode, Sens. Actuators B 182 (2013) 610–617.
[46] Q.L. Sheng, H. Yu, J.B. Zheng, Sol-gel derived carbon ceramic electrode for the investigation of the electrochemical behavior and electrocatalytic activity of neodymium hexacyanoferrate, Electrochim. Acta 52 (2007) 4506–4512.
[47] B.M. Shibuya, M. Miyauchi, Site-selective deposition of metal nanoparticles on aligned WO_3 nanotrees for super-hydrophilic thin films, Adv. Mater. 21 (2009) 1373–1376.

[48] B. Gerand, G. Nowogrocki, J. Guenot, M. Figlarz, Structural study of a new hexagonal from of tungsten trioxide, J. Solid State Chem. 29 (1979) 429–434.
[49] R. Liu, J. Duay, S.B. Lee, Heterogeneous nanostructured electrode materials for electrochemical energy storage, Chem. Commun. 47 (2011) 1384–1404.
[50] T. Zhan, Y. Song, X.J. Li, W.G. Hou, Electrochemical sensor for bisphenol A based on ionic liquid functionalized Zn-Al layered double hydroxide modified electrode, Mater. Sci. Eng. C 64 (2016) 354–361.
[51] E. Laviron, Adsorption, autoinhibition and autocatalysis in polarography and in linear potential sweep voltammetry, J. Electroanal. Chem. 52 (1974) 355–393.
[52] A.J. Bard, L.R. Faulkner, Electrochemical Methods: Fundamentals and Applications, John Wiley & Sons Inc., 1980, pp. 148–153.
[53] Y.Q. Lin, K.Y. Liu, C.Y. Liu, L. Yin, Q. Kang, L.B. Li, B. Li, Electrochemical sensing of bisphenol A based on polyglutamicacid/amino-functionalised carbon nanotubes nanocomposite, Electrochim. Acta 133 (2014) 492–500.
[54] A. Davydov, The Mechanisms of Heterogeneous Catalytic Reactions, John Wiley & Sons Ltd., 2003, pp. 459–558.
[55] L.L. Zhu, Y.H. Cao, G.Q. Cao, Electrochemical sensor based on magneticmolecularly imprinted nanoparticles at surfactant modified magnetic electrode for determination of bisphenol A, Biosens. Bioelectron. 54 (2014) 258–261.
[56] F. Wang, J. Yang, K. Wu, Mesoporous silica-based electrochemical sensor for sensitive determination of environmental hormone bisphenol A, Anal. Chim. Acta 638 (2009) 23–28.
[57] Y.H. Li, X.R. Zhai, X.S. Liu, L. Wang, H.R. Liu, H.B. Wang, Electrochemical determination of bisphenol A at ordered mesoporous carbon modified nano-carbon ionic liquid paste electrode, Talanta 148 (2016) 362–369.
[58] Z. Zheng, Y. Du, Z. Wang, Q. Feng, C. Wang, Pt/graphene–CNTs nanocomposite based electrochemical sensors for the determination of endocrine disruptor bisphenol A in thermal printing papers, Analyst 138 (2013) 693–701.
[59] Y. Uludag, Z. Olcer, M.S. Sagiroglu, Design and characterisation of a thin-film electrode array with shared reference/counter electrodes for electrochemical detection, Biosens. Bioelectron. 57 (2014) 85–90.
[60] X.L. Niu, W. Yang, G.Y. Wang, J. Ren, H. Guo, J.Z. Gao, A novel electrochemical sensor of bisphenol A based on stacked graphene nanofibers/gold nanoparticles composite modified glassy carbon electrode, Electrochim. Acta 98 (2013) 167–175.
[61] Y.Q. Wang, Y.Y. Yang, L. Xu, J. Zhang, Bisphenol A sensing based on surface molecularly imprinted, ordered mesoporous silica, Electrochim. Acta 56 (2011) 2105–2109.
[62] E. Mazzotta, C. Malitesta, E. Margapoti, Direct electrochemical detection of bisphenol A at PEDOT-modified glassy carbon electrodes, Anal. Bioanal. Chem. 405 (2013) 3587–3592.

Biographies

Yuanzhen Zhou is a professor in College of Sciences at Xi'an University of Architecture and Technology. He obtained his Ph. D. in 2007 at the Department of Chemistry of Northwest University, China. His main research interests focus on electroanalytical chemistry and bioelectrochemical sensor.

Lehui Yang is a postgraduate student at Xi'an University of Architecture and Technology, China. Her interests are electroanalytical chemistry and biosensor.

Shanghui Li is a fresh graduate in 2016 from Xi'an University of Architecture and Technology, China.

Yuan Dang obtained her Ph. D. in 2015 at the Department of Chemistry of Northwest University, China. Her research focuses on material surface modification.